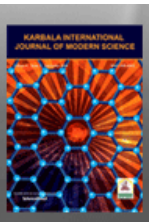

Karbala International Journal of Modern Science

Volume 9 | Issue 2 Article 12

Bio-Colloidal Silver Nanoparticles Prepared via Green Synthesis Using Sandoricum koetjape Peel Extract for Selective Colorimetry-Based Mercury Ions Detection

Ari Sulistyo Rini
Department of Physics, Universitas Riau, Pekanbaru, Indonesia, ari.sulistyo@lecturer.unri.ac.id

Anggrid Fitrisia
Department of Physics, Universitas Riau, Pekanbaru, Indonesia

Yolanda Rati
Department of Physics, Institut Teknologi Bandung, Bandung, Indonesia

Lazuardi Umar
Department of Physics, Universitas Riau, Pekanbaru, Indonesia

Yan Soerbakti
Department of Physics, Universitas Riau, Pekanbaru, Indonesia

Recommended Citation

Rini, Ari Sulistyo; Fitrisia, Anggrid; Rati, Yolanda; Umar, Lazuardi; and Soerbakti, Yan (2023) "Bio-Colloidal Silver Nanoparticles Prepared via Green Synthesis Using Sandoricum koetjape Peel Extract for Selective Colorimetry-Based Mercury Ions Detection," *Karbala International Journal of Modern Science*: Vol. 9 : Iss. 2 , Article 12.
Available at: https://doi.org/10.33640/2405-609X.3299

Bio-Colloidal Silver Nanoparticles Prepared via Green Synthesis Using Sandoricum koetjape Peel Extract for Selective Colorimetry-Based Mercury Ions Detection

Abstract

Hazardous waste from mercury is a critical problem that requires serious attention. Herein, we report bio-colloidal silver nanoparticles (AgNPs) synthesized via green synthesis route from AgNO3 aqueous solution and Sandoricum koetjape (SK) peel extract and demonstrate their sensitivity at detecting mercury ions (Hg2+) using colorimetry. AgNPs were synthesized by varying the volume ratio of AgNO3 solution to SK peel extract, namely AgNPs(4:1), AgNPs(3:2), AgNPs(1:1), AgNPs(2:3), and AgNPs(1:4). Bio-colloidal AgNPs were tested for their ability to detect toxic heavy metal mercury ion by adding different concentrations of Hg2+. All samples have successfully detected Hg2+ at varying levels of sensitivity. This investigation revealed that AgNPs(4:1) is the most sensitive colloid for detecting Hg2+ up to a concentration of 1 ppm.

Keywords

Bio-colloidal; Colorimetric; Mercury ions; Sandoricum koetjape; Silver nanoparticles

RESEARCH PAPER

Bio-Colloidal Silver Nanoparticles Prepared via Green Synthesis Using *Sandoricum koetjape* Peel Extract for Selective Colorimetry-Based Mercury Ions Detection

Ari S. Rini [a,*], Anggrid Fitrisia [a], Yolanda Rati [b], Lazuardi Umar [a], Yan Soerbakti [a]

[a] Department of Physics, Universitas Riau, Pekanbaru, Indonesia
[b] Department of Physics, Institut Teknologi Bandung, Bandung, Indonesia

Abstract

Hazardous waste from mercury is a critical problem that requires serious attention. Herein, we report bio-colloidal silver nanoparticles (AgNPs) synthesized via green synthesis route from $AgNO_3$ aqueous solution and *Sandoricum koetjape* (SK) peel extract and demonstrate their sensitivity at detecting mercury ions (Hg^{2+}) using colorimetry. AgNPs were synthesized by varying the volume ratio of $AgNO_3$ solution to SK peel extract, namely AgNPs(4:1), AgNPs(3:2), AgNPs(1:1), AgNPs(2:3), and AgNPs(1:4). Bio-colloidal AgNPs were tested for their ability to detect toxic heavy metal mercury ion by adding different concentrations of Hg^{2+}. All samples have successfully detected Hg^{2+} at varying levels of sensitivity. This investigation revealed that AgNPs(4:1) is the most sensitive colloid for detecting Hg^{2+} up to a concentration of 1 ppm.

Keywords: Bio-colloidal, Colorimetric, Mercury ions, *Sandoricum koetjape*, Silver nanoparticles

1. Introduction

Mercury is the most toxic heavy metal that naturally occurs in small amounts on earth. Human activities such as battery and electronic devices waste disposal, the manufacturing industry, and gold mining have contributed to the increase in levels of mercury ions (Hg^{2+}) in soil and aquatic ecosystems [1]. Ingestion of mercury by humans will increase the risk of kidney, brain, and lung damage [2,3]. Excessive levels of heavy metal mercury ions can seriously harm human health, pollute the land and water, and represent a big threat to the environment. Therefore, a technique for detecting Hg^{2+} in the environment is urgently needed. The available techniques for determining Hg^{2+} concentrations in the environment include vapor atomic fluorescence spectroscopy [4], high-performance liquid chromatography [5], and inductively coupled plasma mass spectrometry [6]. However, these methods are not efficient due to the difficult and time-consuming process as well as costly [7,8]. The colorimetric method is an effective way of detecting Hg^{2+} by changing the color of the indicator when reacted with the analyte. In addition, the detection process with this method is simple and fast and also produces high sensitivity [9–11].

Colorimetric indicators using silver nanoparticles (AgNPs) have proven to be promising materials for monitoring Hg^{2+} levels. It is due to their high efficiency of surface plasmon resonance (SPR) [2,12]. AgNPs have great optical properties than gold nanoparticles. It has received more attention regarding color changes with visible SPR [13]. AgNPs have high electrical and thermal conductivity, chemical stability, and catalytic activity. In addition, AgNPs also exhibit a broad spectrum of bactericidal and fungicidal activity which makes

Received 24 December 2022; revised 16 March 2023; accepted 21 March 2023.
Available online 5 May 2023

* Corresponding author.
E-mail address: ari.sulistyo@lecturer.unri.ac.id (A.S. Rini).

https://doi.org/10.33640/2405-609X.3299

them very popular in various products including plastics, soaps, pastes, food, and textiles [14,15].

AgNPs can be synthesized through three approaches, namely physics, chemistry, and biology. The synthesis of nanoparticles by physical and chemical methods acquires toxic compounds. Also, the processing techniques are complicated, time-consuming, expensive, and require sophisticated working conditions [13,16]. Thus, biological methods are developing as an environmentally friendly alternative to produce non-toxic nanoparticles with low cost and low energy consumption [14,17]. In general, green synthesis or biosynthesis is the biological method for preparing nanoparticles involving microorganisms, plants, and viruses. Biosynthesis using microbes is less efficient because the breeding process requires complicated procedures and is prone to contamination. Meanwhile, the use of plant extracts can overcome the problem of environmental pollution, is more cost-effective, and has tremendous potential in heavy metal detoxification [18]. The existence of phytochemical substances, primary and secondary metabolites which are responsible for reducing metal salts, drives the use of plant extract for the synthesis of nanoparticles [19,20].

In this paper, we discussed the biological synthesis of AgNPs using the peel extract of sentul fruit or in Latin it is *Sandoricum koetjape* (SK) as a reducing agent. This extract was chosen because SK has high antioxidant activity. In addition, sentul fruit is a tropical fruit native to Southeast Asia which is located in maritime areas such as Indonesia, Malaysia, Philippines, Brunei Darussalam, and Timor-Leste [21]. The synthesized AgNPs were used as a selective colorimetric sensor to investigate the presence of Hg^{2+}. The optical properties, functional group, morphology, and structure of AgNPs will also be discussed based on UV–Vis spectroscopic, Fourier-transform infrared spectroscopy (FTIR), X-ray diffraction (XRD), and transmission electron microscopy (TEM).

2. Experimental details

2.1. Materials

The materials used were freely available and purchased for experimental work. Organic materials such as SK peel are obtained directly from fruit that falls from SK trees which are widespread around the University of Riau, Pekanbaru, Indonesia. The chemicals used included silver nitrate ($AgNO_3$) (EMSURE®) as a silver precursor, sodium hydroxide (NaOH) (EMSURE®) as a stabilizing agent, mercury (II) chloride ($HgCl_2$) (Smart Lab) as an oxidizing agent in colorimetric method, distilled water, and acetone as a solvent, all of which were purchased from Kimia Pro Analyze, East Jakarta, Indonesia.

2.2. Synthesis of bio-colloidal AgNPs

A 20 g/L of SK peel extract was prepared by dissolving 5 g of SK peel powder that has been through the processes of sterilization, drying, and blending into 250 mL of DI water. The biosynthesis of AgNPs was produced by adding $AgNO_3$ solution 2.5 mM to SK peel extract in a 50 mL glass beaker. Then, NaOH was dropped as a catalyst until reached pH 10. These mixtures were heated for 30 min at 80 °C until bio-colloidal AgNPs were formed. In this work, the volume ratio of $AgNO_3$:SK was varied with samples name AgNPs(4:1), AgNPs(3:2), AgNPs(1:1), AgNPs(2:3), and AgNPs(1:4). The schematic procedure of synthesis AgNPs can be seen in Fig. 1.

2.3. Characterizations

UV–Vis spectroscopy analysis was carried out using an Agilent Cary 60 UV–Vis spectrophotometer (Agilent Technologies, Malaysia, G68860A) to determine the peak absorbance of nanoparticles. Functional groups that describe the type of bonding structure of the sample were characterized using FTIR. The crystal structure was examined using an X'Pert-type diffractometer. The morphology of AgNPs was observed using Tecnai-20F Lorentz TEM.

2.4. Colorimetric-based mercury ions detection

A sensitivity test of AgNPs to Hg^{2+} was carried out by adding 1 mL of $HgCl_2$ solution into 0.5 mL of synthesized AgNPs solution into vials. The $HgCl_2$ was prepared in different concentrations of 1, 20, 40, 60, 80, 100, 150, 200, and 250 ppm. The concentrations determine the limits of the detection ability of AgNPs as indicator colorimetry. The color change of the solution was observed (see Fig. 1) and the absorbance was measured using a UV–Vis spectrophotometer.

3. Results and discussion

3.1. Optical properties

UV–Vis absorbance measurement was carried out on a mixture of $AgNO_3$ solution and SK peel extract at various volume ratios. The absorbance spectrum in Fig. 2 shows the SPR peak which corresponds to the characteristics of AgNPs at a wavelength of 407 nm [22].

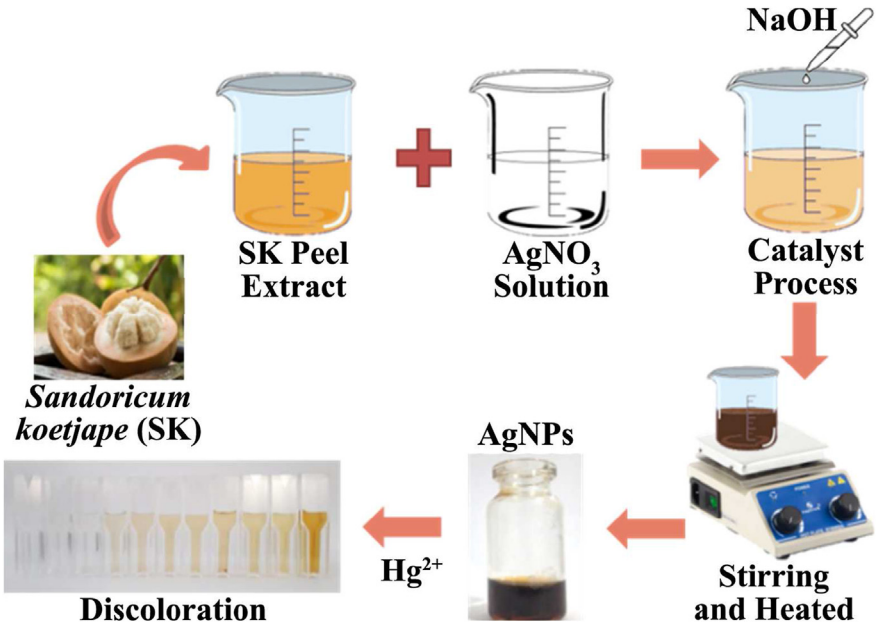

Fig. 1. The biological synthesis scheme of AgNPs.

The color change shows a reduction process for silver ions (Ag^{+}) to form Ag due to the SK peel extract acts as a reducing agent [23]. The SPR peak confirms the effect of SK peel extract volume in reducing Ag^{+} to AgNPs from $AgNO_3$ [14]. The absorbance peak decreases as the volume ratio of $AgNO_3$ reduces. The shift of the absorbance peak occurs towards a wavelength greater than 400 nm which is known as the SPR redshift. In addition, there are also other peaks in the wavelength of less than 350 nm which indicates the effect of SK peel extract compound. It is caused by the electronic transition of the metal Ag appearing in the spectral range of 250–330 nm previously reported using the Gum karaya extract [24].

3.2. FTIR analysis

Fig. 3 depicts the FTIR spectrum used to identify the functional groups present in a sample of AgNPs(1:1) and pure extract of SK peel. The spectrum consists of aromatic (C–H), alkene (C=C),

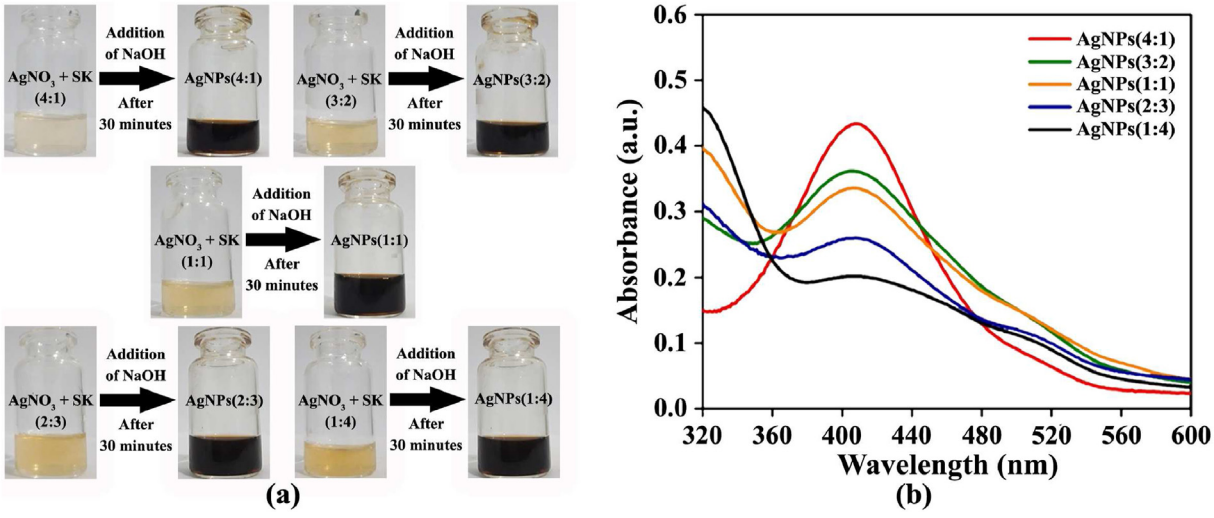

Fig. 2. Several samples of bio-colloidal AgNPs of various volume ratios of $AgNO_3$:SK had uniform visual color as shown in (a), and UV–Vis absorption characteristics as shown in (b) where each sample exhibited an SPR peak in the range of 405–407 nm indicating the formation of the AgNPs structure.

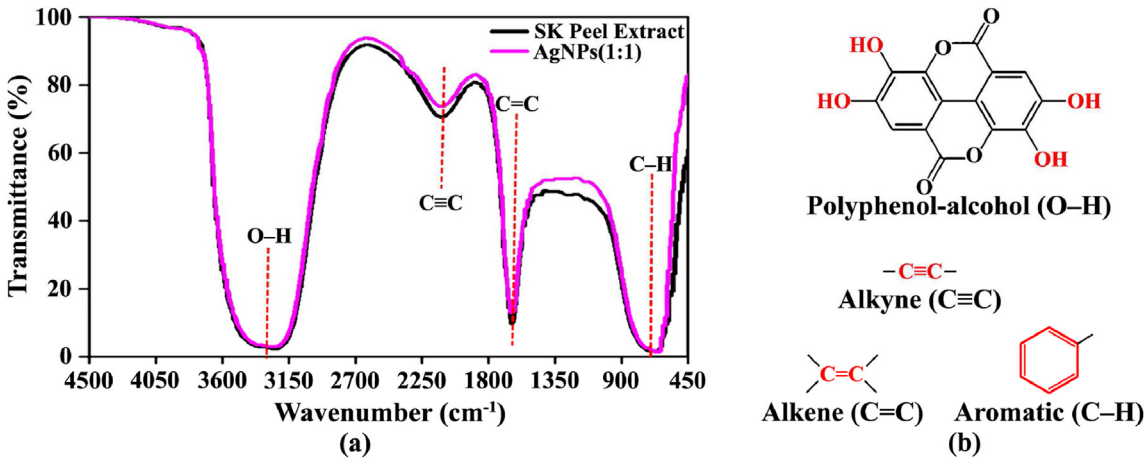

Fig. 3. The minimum FTIR spectrum shows the characteristics of functional groups for SK peel extract samples and AgNPs(1:1) as shown in (a), and the general structure of several identified functional groups as shown in (b) except for the specific polyphenol-alcohol form only arose from the Rosidae subclass in the SK peel extract.

alkyne groups (C≡C), and polyphenol-alcohol (O–H). AgNPs(1:1) sample and SK peel extract have the same functional groups. Each group has a different number range which is shown in Table 1.

The standard for determining the functional groups and bonds of the sample was compared with data from the literature [25]. Both samples have at most 4 functional groups with the smallest wavenumbers in the range of 632–720 cm^{-1} and 641–711 cm^{-1}. The alkene group is shown in the spectral region 1619–1638 cm^{-1} and 1617–1642 cm^{-1}. The alkene group derived from SK peel extract can reduce and act as a stabilizer of Ag^{+} to Ag. It has similarities based on the results of FTIR characterization of AgNPs of red dragon fruit peel extract [25]. The alkene groups can encapsulate AgNPs and bind to metals to prevent particle agglomeration [26]. The IR absorbance at the wavenumber ranges of 2110–2135 cm^{-1} and 2108 cm^{-1} show the connection between alkyne functions. Absorbance at the wavenumber ranges of 3204–3481 cm^{-1} and 3179–3575 cm^{-1}, shows polyphenol-alcohol in AgNPs (1:1) and SK peel extract.

Table 1. Infrared spectrum data from FTIR analysis.

Wavenumber (cm^{-1})		Functional Group	Chemical Bond
AgNPs(1:1)	SK Peel Extract		
632–720	641–711	Aromatic	C–H
1619–1638	1617–1642	Alkene	C=C
2110–2135	2108	Alkyne	C≡C
3204–3481	3179–3575	Polyphenol-Alcohol	O–H

3.3. Structural analysis

XRD investigation revealed the crystalline nature of Ag nanoparticles. The XRD pattern of dried nanoparticles derived from colloid samples is shown in Fig. 4. The XRD peaks show Bragg reflections at diffraction angles of 38.36°, 44.06°, 64.72°, and 77.42° indicating the (111), (200), (220), and (311) planes of silver, respectively. The peaks are consistent with the crystalline phase of the face-centered cubic structure and agree with the standard powder diffraction card of JCPDS, silver file no. 04-0783 [27].

The observed peak broadening was most likely caused by macromolecules contained in the plant extract, which might be responsible for silver ion reduction. As a result, the XRD pattern clearly showed that the silver nanoparticles produced in this current synthesis are crystalline in nature. There are additional peaks detected in addition to the Bragg peaks that represent silver nanocrystals, showing that bio-organic phase crystallization occurs on the surface of the silver nanoparticles [28]. This peak is denoted by an asterisk (*).

The structure information, such as crystallite size (D), the distance between crystal planes, and lattice constant (a) were determined using Debye–Scherrer formula in Equation (1), Bragg formula in Equation (2), and formulation lattice constant on the cubic-type system in Equation (3), respectively.

$$D = \frac{0.9\lambda}{\beta \cos\theta} \quad (1)$$

$$2d_{hkl} \sin\theta = n\lambda \quad (2)$$

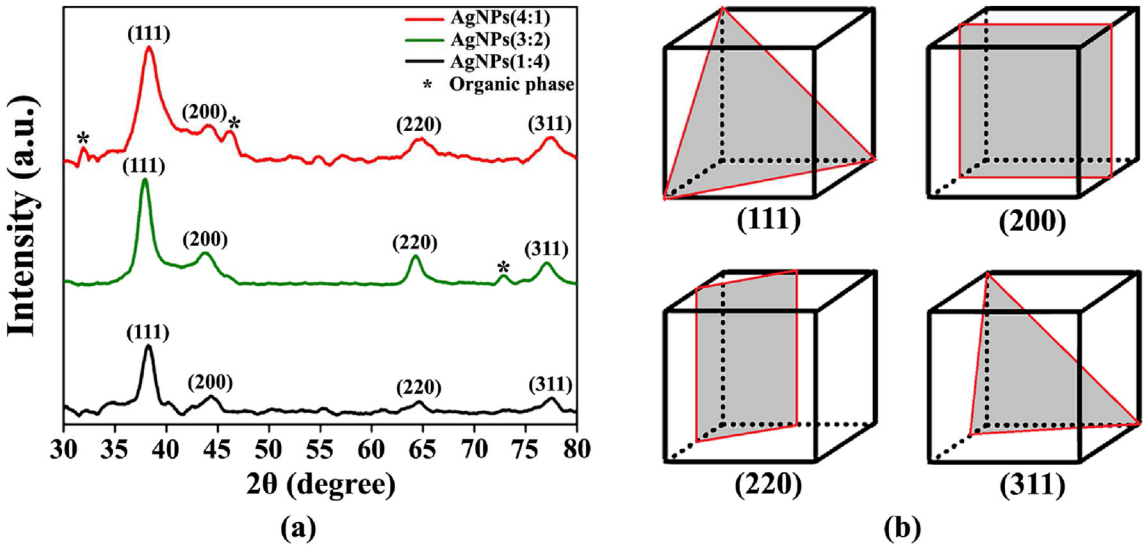

Fig. 4. The XRD spectra of each AgNPs sample show the presence of a crystal lattice shape and the diffraction angle at the peaks is almost the same as that shown in (a), and the crystal lattice plane representation of each AgNPs sample as in (b) shows its consistency with the face-centered cubic structure.

$$a = d \times \sqrt{h^2 + k^2 + l^2} \quad (3)$$

where, λ is the wavelength of X-ray (1.5406 Å), β is the full width at half maximum (FWHM), θ is the diffraction angle, d_{hkl} is the interplanar spacing, and hkl is the Miller indices [29]. The XRD parameters including the lattice parameter and crystal sizes are shown in Table 2.

The sample with the highest crystal size is AgNPs(3:2) in the (111) and (311) planes of 6.906 nm and 7.488 nm, respectively. Meanwhile, the planes (200) and (220) are found in the AgNPs(1:4) sample. These samples have the largest crystal sizes of 5.998 nm and 10.92 nm, respectively. These crystal sizes include the size standard for AgNPs which are usually 2–10 nm [30]. The average size lattice parameter of nanoparticles was calculated at 4.086 nm. The estimated lattice constant is in accordance with the previously reported [31].

3.4. Morphology of AgNPs

Fig. 5 displays the morphology and particle size histogram of the AgNPs samples. The TEM image revealed that the majority of the particles generated by AgNPs were spherical, with some being oval. This particle form is identical to what has been observed in earlier research utilizing *Citrullus lanatus* peel extract [32]. AgNPs synthesized by biological systems tend to have a similar shape and size [33].

Particles in AgNPs(4:1) appear to have the smallest size while the largest particle size is obtained at AgNPs(1:4). These results are in accordance with the

Table 2. Characteristic XRD parameters of AgNPs.

Sample	Plane (*hkl*)	2θ (degree)	FWHM (degree)	Crystallite Size (nm)	Interplanar Spacing (nm)	Lattice Parameter (nm)
AgNPs(4:1)	(111)	38.37	1.659	5.070	2.344	4.060
	(200)	44.06	1.821	4.705	2.054	4.107
	(220)	64.72	1.391	6.763	1.439	4.070
	(311)	77.42	1.684	6.046	1.232	4.085
AgNPs(3:2)	(111)	37.94	1.216	6.906	2.370	4.105
	(200)	43.78	1.728	4.956	2.066	4.130
	(220)	64.30	1.247	7.526	1.447	4.094
	(311)	77.06	1.356	7.488	1.237	4.101
AgNPs(1:4)	(111)	38.24	1.264	6.653	2.352	4.073
	(200)	44.32	1.430	5.998	2.042	4.084
	(220)	64.58	0.861	10.92	1.442	4.079
	(311)	77.44	1.615	6.305	1.232	4.084

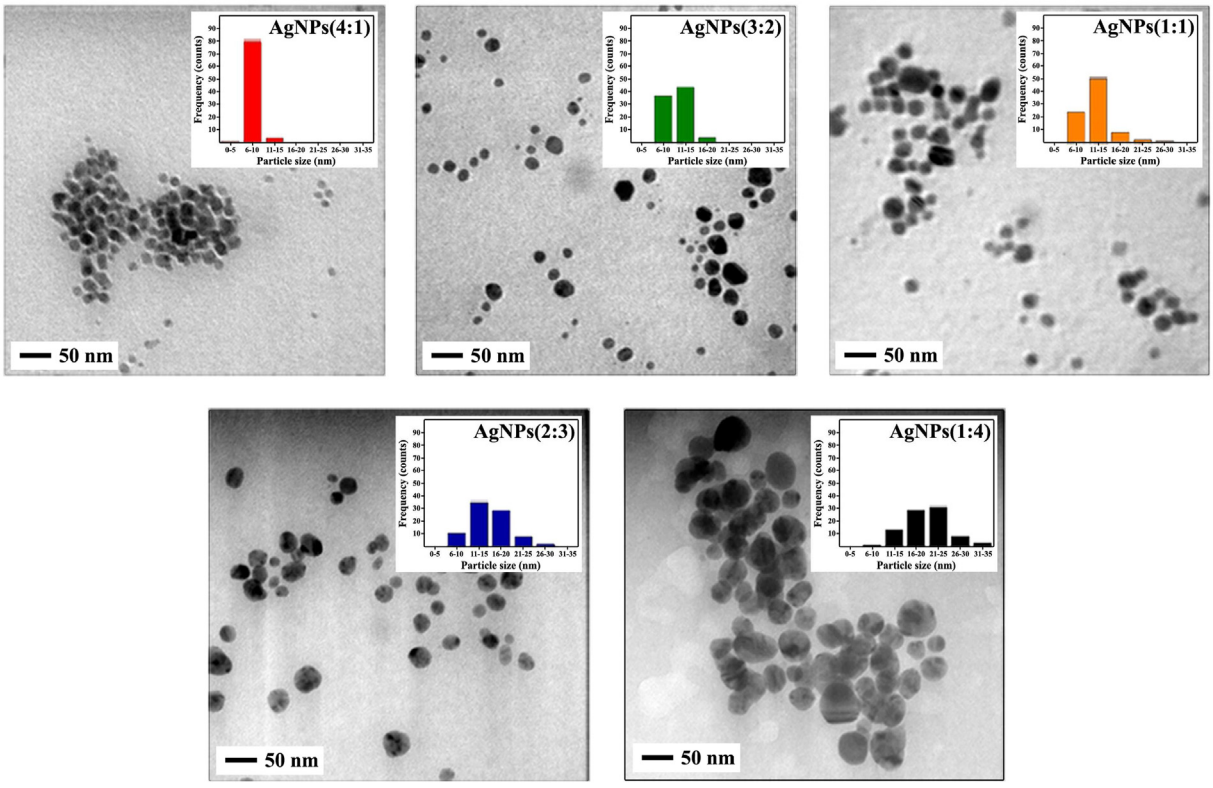

Fig. 5. Morphology and histogram of AgNPs with variations in volume ratio.

SPR band from UV–Vis spectroscopic characterization. The absorption peak at lower wavelengths indicates a smaller size of AgNPs formed, while higher wavelengths indicate a larger size of AgNPs formed [34]. In addition, the difference in particle size is also caused by the volume used where the larger the volume of $AgNO_3$ in the sample, the smaller the particle size. The distribution of particle sizes in each sample is shown in the histogram graph inserted in Fig. 5. The decrease in the volume of $AgNO_3$ resulted in a more uneven distribution of particle size as seen from the larger standard deviation value. It means the sample with the highest SPR peak has an even distribution of particle size.

3.5. High-sensitivity mercury ions detection

The sensitivity of AgNPs to detect Hg^{2+} with varying concentrations of $HgCl_2$ can be seen from the UV–Vis spectrum in Fig. 6. Detection of Hg^{2+} was determined from the SPR peak of AgNPs. It can be seen that the SPR peak decreases with increasing Hg^{2+} concentration. A blue shift occurs at the absorption peak of the AgNPs curve from 407 nm to 384 nm due to an increase in the concentration of $HgCl_2$. This phenomenon indicates that the distance between nanoparticles gets closer during the reduction of $HgCl_2$ by AgNPs. So, the frequency increases and at the same time shortens the wavelength [7].

The reaction of AgNPs and $HgCl_2$ produces a color change which indicates the ability of the AgNPs sensor to detect the presence of Hg^{2+}. AgNPs(4:1) after reacted changed color from yellowish brown to pale yellow to a concentration of 150 ppm which was observed for 30 min. The color of the reaction degraded and turned colorless gradually with increasing concentration of $HgCl_2$ and finally same to water. This sample shows a significant color change compared to other AgNPs samples. AgNPs(3:2), AgNPs(1:1), and AgNPs(2:3) showed a less significant change in the color of the reaction products. It was the highest concentration of $HgCl_2$ resulting in a change in the color only to pale yellow. In addition, the AgNPs(1:4) also produced an insignificant change where the final color change at the largest concentration of $HgCl_2$ of the bio-colloidal AgNPs to a solid yellow color limit. It is supported by the highest absorbance peak in the AgNPs(4:1) where the SPR properties are better. The resulting color change corresponds to the SPR properties of AgNPs with an increase in the

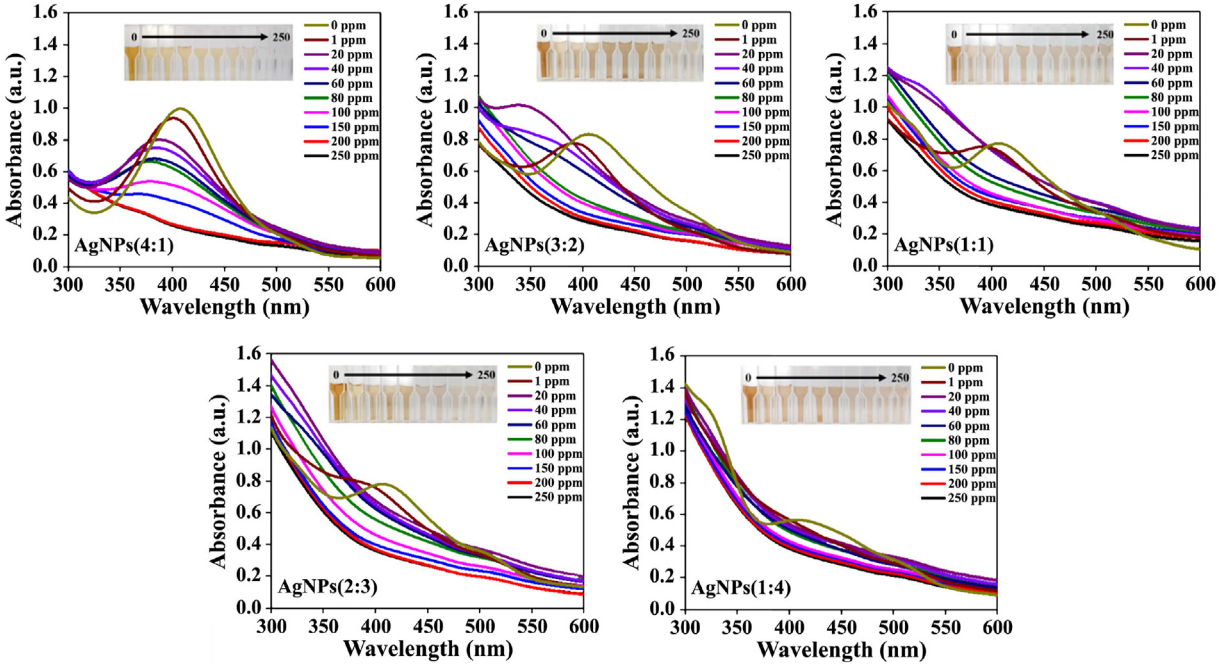

Fig. 6. UV–Vis spectra of AgNPs using different concentrations of Hg^{2+}.

concentration of $HgCl_2$ which can be seen clearly. In addition, bio-colloidal AgNPs change color due to aggregation by the Hg analyte and due to the strongly oxidizing properties of $HgCl_2$. Color loss occurs due to the release of Ag^+ and subsequent reactions with Cl^- to form AgCl [35].

AgNPs(4:1) in Fig. 6 shows a significant decrease and widening of the absorption peak of the SPR band with an increase in the concentration of $HgCl_2$. This result is associated with a significant color change. SPR curve at AgNPs(3:2) (Fig. 6) which experienced a significant decrease occurred only at concentrations of $HgCl_2$ from 1 to 80 ppm. Meanwhile, the larger concentration only decreased slowly indicated by the adjacent curve. The same results were also found in the AgNPs(1:1), AgNPs(2:3), and AgNPs(1:4) (Fig. 6) which the SPR curve experienced a significant decrease only to $HgCl_2$ concentrations of 60 ppm, 20 ppm, and 1 ppm, respectively. At large concentrations, there is only a slight decrease in the curve. The SPR curves for large $HgCl_2$ concentrations appear to coincide. It indicates there is no more change in the color of the solution. From these results, it can be seen that increasing the volume ratio of the extract reduces the mercury ions detection ability in AgNPs. So, AgNPs(4:1) is considered the most sensitive sample in detecting mercury ions compared to other either from a change in color solution and optical absorption.

The linear relationship between absorbance intensity and $HgCl_2$ concentration is shown in Fig. 7. The regression value for AgNPs(4:1), AgNPs(3:2), AgNPs(1:1), AgNPs(2:3), and AgNPs(1:4) samples are 0.9141, 0.8337, 0.8357, 0.8325, and 0.9094, respectively. The greatest regression value was obtained at AgNPs(4:1) with a steep slope. AgNPs(3:2) and AgNPs(1:1) also have a steep slope but the regression value obtained is lower. AgNPs(2:3) and AgNPs(1:4) regression values obtained are quite large but the slope of the linear line is very small. Based on these results, AgNPs(4:1) can be concluded as the most sensitive sample to Hg^{2+} in colorimetric detection. Overall, the absorbance of AgNPs decreased with increasing Hg^{2+} concentration. It indicates AgNPs sample synthesized with the bio-reductant of SK peel extract can be used as a colorimetric sensor for mercury ions. The redox reaction is the principle of colorimetric detection of mercury ions by AgNPs. Most of the transition metals, alkalis, and alkaline earth metals cannot oxidize Ag from AgNPs to Ag^+ due to their lower reduction potential than Ag^+. Therefore, it enables highly selective analysis of Hg^{2+}. Hg^{2+} has a higher reduction potential than Ag^+, so the redox reactions that occur can be seen in Equation (4) [6].

$$2Ag + Hg^{2+} \rightarrow 2Ag^+ + Hg \quad (4)$$

Oxidation of Ag to Ag^+ changes the color of AgNPs from yellowish brown to colorless, as observed in the initial colorless $AgNO_3$ solution.

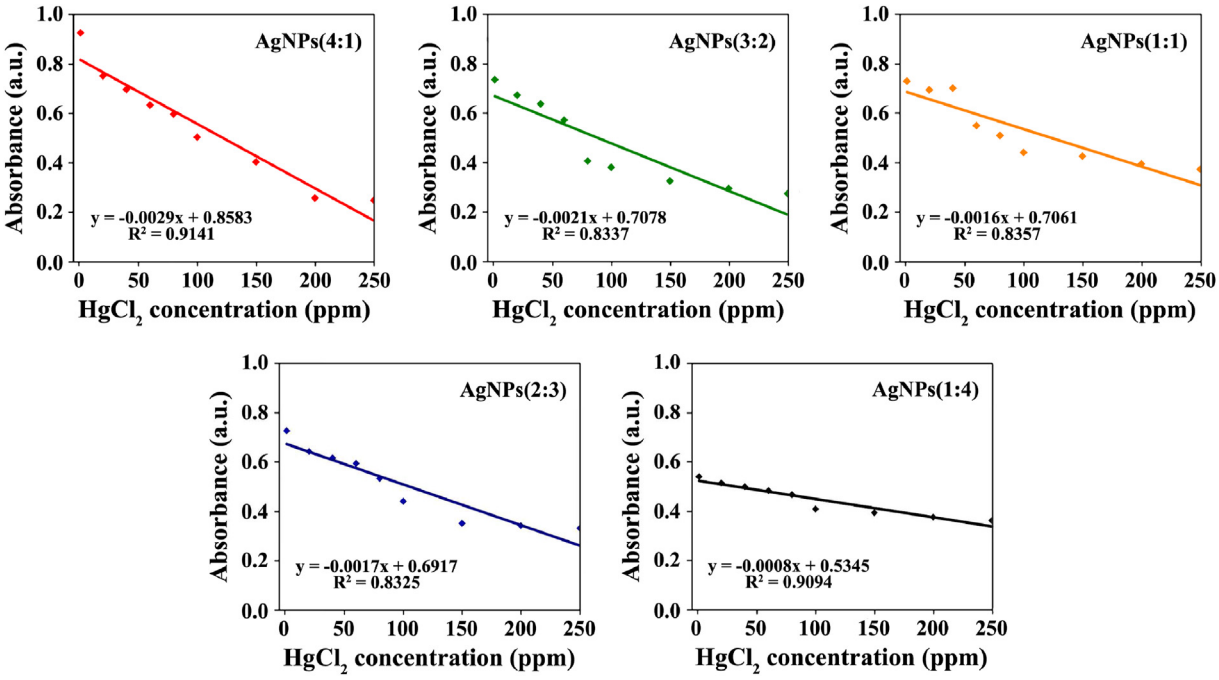

Fig. 7. The plot of absorbance intensity at 407 nm versus Hg^{2+} concentration.

4. Conclusions

The green synthesis approach is cost-effective and environmentally benign to produce AgNPs. Here, the SK peel extract acts as both a reducing and stabilizing agent. The surface plasmon resonance of green-synthesized silver nanoparticles confirmed the existence of AgNPs. The results of X-ray diffraction demonstrate clearly that the silver nanoparticles generated by the reduction of Ag^{+} ions by the extract of SK peel are crystalline in nature. Using Debye- Scherrer's formula, the average crystalline size of AgNPs is calculated to be less than 10 nm. The particle size of AgNPs from TEM was found to be less than 20 nm. This study demonstrated that AgNPs are highly sensitive colorimetric sensors for detecting Hg^{2+} due to their ability to induce large colloid color changes.

Acknowledgment

This work is funded by the Ministry of Education, Culture, Research, and Technology, Republic of Indonesia under year 2022 research grant. The authors also would like to thank the Lembaga Penelitian dan Pengabdian Masyarakat (LPPM), University of Riau, for supporting this research.

References

[1] D.R. Rotake, A. Kumar, A.D. Darji, J. Singh, Highly selective sensor for the detection of Hg^{2+} ions using homocysteine functionalised quartz crystal microbalance with cross-linked pyridinedicarboxylic acid, IET Nanobiotechnol 14 (2020) 563–573, https://doi.org/10.1049/iet-nbt.2020.0109.

[2] M.O.S. Lobregas, J.P.O. Bantang, D.H. Camacho, Carrageenan-stabilized silver nanoparticle gel probe kit for colorimetric sensing of mercury (II) using digital image analysis, Sens Bio-Sens Res 26 (2019) 1–9, https://doi.org/10.1016/j.sbsr.2019.100303.

[3] R. Pamphlett, The prevalence of inorganic mercury in human cells increases during aging but decreases in the very old, Sci Rep 11 (2021) 1–8, https://doi.org/10.1038/s41598-021-96359-8.

[4] D.G. da Silva, L.A. Portugal, A.M. Serra, S.L.C. Ferreira, V. Cerdà, Determination of mercury in rice by MSFIA and cold vapour atomic fluorescence spectrometry, Food Chem 137 (2013) 159–163, https://doi.org/10.1016/j.foodchem.2012.10.019.

[5] M. Laosuwan, S. Mukdasai, S. Srijaranai, A simple in syringe low density solvent-dispersive liquid liquid microextraction for enrichment of some metal ions prior to their determination by high performance liquid chromatography in food samples,, Molecules 25 (2020) 1–13, https://doi.org/10.3390/molecules25030552.

[6] B. Song, H. He, L. Chen, S. Yang, Y. Yongguang, Y. Li, Speciation of mercury in microalgae by isotope dilution-inductively coupled plasma mass spectrometry, Anal Lett 50 (2017) 2161–2176, https://doi.org/10.1080/00032719.2016.1269119.

[7] M.L. Firdaus, I. Fitriani, S. Wyantuti, Y.W. Hartati, R. Khaydarov, J.A. Mcalister, H. Obata, T. Gamo, Colorimetric detection of mercury(II) ion in aqueous solution using silver nanoparticles, Anal Sci 33 (2017) 831–837, https://doi.org/10.2116/analsci.33.831.

[8] G. Peng, Y. Chen, R. Deng, Q. He, D. Liu, Y. Lu, J.M. Lin, Highly sensitive and selective determination of Hg (II) based on microfluidic chip with on-line fluorescent derivatization, Spectrochim Acta Mol Biomol Spectrosc 204 (2018) 1–6, https://doi.org/10.1016/j.saa.2018.06.006.

[9] A. Mohtasebi, A.D. Broomfield, T. Chowdhury, P.R. Selvaganapathy, P. Kruse, Reagent-free quantification of aqueous free chlorine via electrical readout of colorimetrically

functionalized pencil lines, ACS Appl Mater Interfaces 9 (2017) 20748–20761, https://doi.org/10.1021/acsami.7b03968.
[10] M.R. Awual, Novel nanocomposite materials for efficient and selective mercury ions capturing from wastewater, Chem Eng J 307 (2017) 456–465, https://doi.org/10.1016/j.cej.2016.08.108.
[11] M.R. Awual, An efficient composite material for selective lead (II) monitoring and removal from wastewater, J Environ Chem Eng 7 (2019) 103087, https://doi.org/10.1016/j.jece.2019.103087.
[12] K. Zhang, Y. Sang, Y. Gao, Q. Sun, W. Li, A fluorescence turn-on CDs-AgNPs composites for highly sensitive and selective detection of Hg^{2+}, Spectrochim, Acta A Mol Biomol Spectrosc 264 (2022) 1–8, https://doi.org/10.1016/j.saa.2021.120281.
[13] J.A. Aboyewa, N.R.S. Sibuyi, M. Meyer, O.O. Oguntibeju, Green synthesis of metallic nanoparticles using some selected medicinal plants from southern africa and their biological applications, Plants 10 (2021) 1–24, https://doi.org/10.3390/plants10091929.
[14] K. Ponsanti, B. Tangnorawich, N. Ngernyuang, C. Pechyen, A flower shape-green synthesis and characterization of silver nanoparticles (AgNPs) with different starch as a reducing agent,, J Mater Res Technol 9 (2020) 11003–11012, https://doi.org/10.1016/j.jmrt.2020.07.077.
[15] S.P. Mahaparale, R.S. Kore, Silver nanoparticles: synthesis, characterization, application, future outlook, Asian J Pharmaceut Res 9 (2019) 181–189, https://doi.org/10.5958/2231-5691.2019.00029.7.
[16] N. Sarfraz, I. Khan, Plasmonic gold nanoparticles (AuNPs): properties, synthesis and their advanced energy, environmental and biomedical applications, Chem Asian J 16 (2021) 720–742, https://doi.org/10.1002/asia.202001202.
[17] A. Aminu, S.A. Oladepo, Fast orange peel-mediated synthesis of silver nanoparticles and use as visual colorimetric sensor in the selective detection of mercury (II) ions, Arab J Sci Eng 46 (2021) 5477–5487.
[18] C. Verma, E.E. Ebenso, I. Bahadur, M.A. Quraishi, An overview on plant extracts as environmental sustainable and green corrosion inhibitors for metals and alloys in aggressive corrosive media, J Mol Liq 266 (2018) 577–590, https://doi.org/10.1016/j.molliq.2018.06.110.
[19] W. Wubet, Green synthesis of CuO nanoparticles for the application of dye sensitized solar cell, World J Pharmaceut Res 9 (2020) 29–51, https://doi.org/10.20959/wjpr202013-18436.
[20] A.S. Rini, N. Hidayanti, Y. Rati, Biosynthesis of zinc oxide powder using *Sandoricum koetjape* peel extract at various annealing temperature, Positron 11 (2021) 57–62, https://doi.org/10.26418/positron.v11i2.49699.
[21] F.N. Hamzah, Subandi, W. Sujarwo, A.W. Septama, T. Mozef, Antioxidant and xanthine oxidase inhibitory activities of Kecapi *(Sandoricum koetjape (Burm.f) Merr.)* leaf extract, IOP Conf Ser Mater Sci Eng 833 (2020) 1–8, https://doi.org/10.1088/1757-899X/833/1/012012.
[22] R. Baber, L. Mazzei, N.T.K. Thanh, A. Gavriilidis, An engineering approach to synthesis of gold and silver nanoparticles by controlling hydrodynamics and mixing based on a coaxial flow reactor, Nanoscale 9 (2017) 14149–14161, https://doi.org/10.1039/c7nr04962e.
[23] K. Alaqad, T.A. Saleh, Gold and silver nanoparticles: synthesis methods, characterization routes and applications towards drugs, J Environ Anal Toxicol 6 (2016) 1–10, https://doi.org/10.4172/2161-0525.1000384.
[24] M. Venkatesham, D. Ayodhya, A. Madhusudhan, A. Santoshi Kumari, G. Veerabhadram, K.G. Mangatayaru, A novel green synthesis of silver nanoparticles using gum karaya: characterization, antimicrobial and catalytic activity studies, J Cluster Sci 25 (2014) 409–422, https://doi.org/10.1007/s10876-013-0620-1.
[25] S. Phongtongpasuk, S. Poadang, N. Yongvanich, Environmental-friendly method for synthesis of silver nanoparticles from dragon fruit peel extract and their antibacterial activities, Energy Proc 89 (2016) 239–247, https://doi.org/10.1016/j.egypro.2016.05.031.
[26] G.B. Sheik, A.I.A.A. Raheim, Z.A. Alzeyadi, M.I. AlGhonaim, Extracellular synthesis, characterization and antibacterial activity of silver nanoparticles by a potent isolate *Streptomyces sp.* DW_{102}, Asian J Biol Life Sci 8 (2019) 89–96, https://doi.org/10.5530/ajbls.2019.8.15.
[27] S. Joseph, B. Mathew, Microwave assisted biosynthesis of silver nanoparticles using the rhizome extract of Alpinia galanga and evaluation of their catalytic and antimicrobial activities, J Nanopart 2014 (2014) 1–9, https://doi.org/10.1155/2014/967802.
[28] A.M. Awwad, N.M. Salem, A.O. Abdeen, Green synthesis of silver nanoparticles using carob leaf extract and its antibacterial activity, Int J Ind Chem 4 (2013) 1–6, https://doi.org/10.1186/2228-5547-4-29.
[29] S.P. Sivagnanam, A.T. Getachew, J.H. Choi, Green synthesis of silver nanoparticles from deoiled brown algal extract via Box-Behnken based design and their antimicrobial and sensing properties, Green Process Synth 6 (2017) 147–160, https://doi.org/10.1515/gps-2016-0052.
[30] P. Kanmani, S.T. Lim, Synthesis and characterization of pullulan-mediated silver nanoparticles and its antimicrobial activities, Carbohydr Polym 97 (2013) 421–428, https://doi.org/10.1016/j.carbpol.2013.04.048.
[31] K. Anandalakshmi, J. Venugobal, V. Ramasamy, Characterization of silver nanoparticles by green synthesis method using *Pedalium murex* leaf extract and their antibacterial activity, Appl Nanosci 6 (2016) 399–408, https://doi.org/10.1007/s13204-015-0449-z.
[32] A.S. Rini, H. Adzani, T.S.L. Husain, M.P. Deraf, Y.Rati, Y. Hamzah, Structural and morphological studies of silver nanoparticles prepared using citrullus lanatus rind extract, AIP Conf Proc 2320 (2021) 1–6, https://doi.org/10.1063/5.0037960.
[33] P. Singh, Y.J. Kim, H. Singh, C. Wang, K.H. Hwang, M.E.A. Farh, D.C. Yang, Biosynthesis, characterization, and antimicrobial applications of silver nanoparticles, Int J Nanomed 10 (2015) 2567–2577, https://doi.org/10.2147/IJN.S72313.
[34] W.K.A.W.M. Khalir, K. Shameli, S.D. Jazayeri, N.A. Othman, N.W. Che Jusoh, N.M. Hassan, Biosynthesized silver nanoparticles by aqueous stem extract of *Entada spiralis* and screening of their biomedical activity, Front Chem 8 (2020) 1–15, https://doi.org/10.3389/fchem.2020.00620.
[35] G.M. Sangaonkar, M.P. Desai, T.D. Dongale, K.D. Pawar, Selective interaction between phytomediated anionic silver nanoparticles and mercury leading to amalgam formation enables highly sensitive, colorimetric and memristor-based detection of mercury, Sci Rep 10 (2020) 1–12, https://doi.org/10.1038/s41598-020-58844-4.